論文

Damping in 2-D Woven and 3-D Braided Textile Structural Composites

Bor Z. Jang* and Jong Hee Yim**

2-D와 3-D 직물복합재료의 댐핑

Bor Z. Jang* · 임종휘**

초 록

2-D와 3-D 직물 구조로된 복합재료의 댐핑 특성이 조사되어왔다. 이들 복합재료를 위한 한 모델이 Kirchoff-Love의 가설하에 18개의 재료 상수로 구성된 고전 적층판 이론과 탄성-점탄성 상응 원리 그리고 이들 직물 복합 재료의 정적 탄성 계수를 예측하는 현존하는 모델들을 근거로 개발되었다. 이들 상수들의 여섯은 [A]로 표시되는 인장 stiffness, 다른 여섯은 [B]로 표시되는 굽힘-인장 연계 stiffness, 나머지 여섯은 [D]로 표시되는 굽힘 stiffness로 묘사되었다. 이론적 댐핑 값들을 평가하기 위하여 먼저 [A], [B], [D]의 storage stiffness는 각각의 적층부의 h_k층의 두께와 $[Q]_k$탄성 상수 매트릭스와 고전 적층판 이론으로 부터 결정 하였다. 거기서 Q_{ij}^k의 성분들을 4개의 기본 공학 상수 E_L, E_T, G_{LT}와 ν_{LT} 에 의해 얻었다. 또한 loss stiffness를 결정하기 위하여 그 기본 공학 상수들은 탄성-점탄성 상응 원리를 사용함으로서 복소수형태의 공학 상수들로 표현하였다. 그 결과로서 신장 댐핑 $A\eta_{ij} = A_{ij}''/A_{ij}'$; 연계 댐핑은 $B\eta_{ij} = B_{ij}''/B_{ij}'$ 그리고 굽힘 댐핑은 $D\eta_{ij} = D_{ij}''/D_{ij}'$로 표현되었다. 본 연구에서 그 기본 댐핑 손실 계수 η_L, η_T, η_{LT}, $\eta_{\nu LT}$들은 수정된 Hashin's 이론과 혼합 법칙에 의해 결정되었다.

수치 해석 결과로 부터 본 연구는 인장 댐핑, 인장-굽힘 댐핑, 굽힘 댐핑과 공학적 댐핑은 2-D 직물구조로된 복합재료에서 n_g(기하학적 형상 계수)의 함수로 나타났다. 또한 3-D 직물 구조로된 복합재료의 인장 댐핑, 평면전단 댐핑과 Poisson's 댐핑은 yarn orientation 각과 섬유 부피율의 함수로 나타났다. 그들의 부분적인 실험 결과는 이론적 예측이 합당한 것으로 확인할수 있었다.

ABSTRACT

Material damping characteristics of 2-D and 3-D textile structural composites were investigated. A model for predicting damping in these materials was developed based upon the classical laminated plate theory. The model entailed 18 material constants and made use of the Kirchoff-Love hypothesis, the elastic-viscoelastic correspondence principle, and some existing models for predicting the static moduli of textile structural composites. These 18 constants included 6 for describing the stretching stiffness matrix represented by [A], another 6 for the bendingstretching coupling stiffness matrix represented by [B], and the other 6 for the bending stiffness matrix represented by [D]. To evaluate the theoretical values of damping, the storage stiffness elements of [A], [B] and [D] were determined by first expressing [A], [B], and [D] in terms

* 미 Auburn University, 재료공학과 교수

** 광주-전남 중소기업청, 시험검사과, 공업연구사

of the stiffness matrix $[Q]_k$ and layer thickness h_k of each lamina. The components of Q_{ij}^K were in turn expressed in terms of the 4 basic engineering constants E_L, E_T, G_{LT} and υ_{LT}. The basic engineering constants were replaced by their corresponding complex moduli by making use of the elastic and viscoelastic correspondence principle: e.g., stretching damping, $A\eta ij = A^*_{ij}/A'_{ij}$; coupling damping, $B\eta_{ij} = B^*_{ij}/B'_{ij}$; and bending damping, $D\eta_{ij} = D^*_{ij}/D'_{ij}$. In this study, the basic damping loss factors η_L, η_T, η_{LT}, $\eta\upsilon_{LT}$ were determined by a modified Hashin's theory and Rule-of-Mixture Laws. From numerical results, we concluded that stretching damping, stretching-bending damping, bending damping and engineering damping coefficients are all functions of ng (a geometric parameter) in 2-D woven textile structural composites. Also, the axial damping, the in-plane shear damping and the in-plane Poisson's damping coefficients are all functions of yarn orientation angle and fiber volume fraction in 3-D braided textile structural composites. Experimental data supported theoretically predicted results.

1. INTRODUCTION

Two-dimensional and three-dimensional textile structural composites have been utilized in applications such as boats, pressure vessels, propellers, turbine blades and horizontal stabilizers. In these applications, damping is an important material property that must be properly considered for design [1-3]. These composites have many advantages over conventional laminated composites and can be used freely to meet various manufacturing requirements such as dimensional stability, stable conformability and deep-draw shapeability. Two-dimensional (2-D) fabric composites provide an improved shear resistance, more balanced properties in the fabric plane and an increased impact resistance due to the bidirectional reinforcement. Ishikawa and Chou [4-6] have proposed a methodology for predicting static elastic constants and strengths of these 2-D fabric composites.

Three-dimensional (3-D) textile structural composites are useful for thick-section applications due to high interlaminar moduli and strength. Several recent efforts [8-11] have been made to investigate the static modulus of 3-D textile structural composites. A model [8], extending classical lamination theory to 3-D braided reinforced composites, may predict accurately the static modulus. However, models that can be used to predict damping in textile structural composites have yet to be proposed. Using existing models for predicting the static moduli of 2-D and 3-D textile structural composites, we have developed a methodology for predicting material damping to increase the design database for these materials.

2. THEORETICAL

2-1. Methodology of Damping Prediction

As a first step, we used the elastic-viscoelastic correspondence principle to obtain the complex moduli. Each complex modulus includes two real constants for storage and loss components. The material damping is obtained as the ratio of the loss modulus to the storage modulus. Using the elastic-viscoelastic correspondence principle [3] we analytically expressed in a complex form the basic engineering constants for material damping of textile structural composites as follows:

$$E_L^* = E_L(1 + i\eta_L) \quad \cdots\cdots (1)$$

$$E_T^* = E_T(1 + i\eta_T) \quad \cdots\cdots (2)$$

$$G_{LT}^* = G_{LT}(1 + i\eta_{LT}) \quad \cdots\cdots (3)$$

$$v_{LT}^* = v_{LT}(1 + i\eta_{vLT}) \quad \cdots\cdots (4)$$

where,

$$\eta_L = \frac{\eta_m V_m}{V_m + V_f(\frac{E_{Lf}}{E_m})^{\alpha}}$$

$$\eta_T = \eta_m - \frac{\eta_m V_f}{V_f + V_m(\frac{E_{Tf}}{E_m})^{\zeta}}$$

$$\eta_{LT} = \frac{\eta_m(1-V_f)[(G+1)^{(2}+\beta)+V_f(G-1)^{(2}+\beta)]}{[G^{(1}+\beta)(1+V_f)+1-V_f][G^{(1}+\beta)(1-V_f)+1+V_f]}$$

$$\eta_{vLT} = \frac{\eta_{vLTf} v_{LTf} V_f + \eta_{vm} v_{LTm} V_m}{V_f v_{LTf} + V_m v_{LTm}}$$

where, V_f = 1- V_m is the fiber volume fraction, α, ζ and β are curve fitting parameters for data reduction, and $G = \frac{G_f}{G_m}$. The relations between Qij and the basic engineering constants are described as

$$Q_{xx} = \frac{E_L}{1-(v_{LT})^2 E_T/E_L} \quad \cdots\cdots (5)$$

$$Q_{xy} = \frac{v_{LT} E_T}{1-(v_{LT})^2 E_T/E_L} \quad \cdots\cdots (6)$$

$$Q_{yy} = \frac{E_T}{1-(v_{LT})^2 E_T/E_L} \quad \cdots\cdots (7)$$

$$Q_{ss} = G_{LT} \quad \cdots\cdots (8)$$

Substituting Eqs.(1)-(4) into Eqs.(5)-(8), we obtained the following relations :

$$Q^*_{xx} = Q'_{xx} + iQ''_{xx} \quad \cdots\cdots (9)$$

$$Q^*_{yy} = Q'_{yy} + iQ''_{yy} \quad \cdots\cdots (10)$$

$$Q^*_{xy} = Q'_{xy} + iQ''_{xy} \quad \cdots\cdots (11)$$

$$Q^*_{ss} = G^*_{LT} = G_{LT}(1 + i\eta_{LT}) \quad \cdots\cdots (12)$$

We transformed [Q] with reference to the fiber orientation of each layer. The transformed $\overline{Q}'_{ij}$ and $\overline{Q}''_{ij}$ (i, j =1, 2, 6) which are related to Qij (i, j =x, y, s) can be written as [14] :

$$\overline{Q}_{11} = Q_{xx}\cos^4\theta + Q_{yy}\sin^4\theta + 2(Q_{xy} + 2Q_{ss})\sin^2\theta\cos^2\theta \quad \cdots\cdots (13)$$

$$\overline{Q}_{26} = (Q_{xx} - Q_{xy} - 2Q_{ss})\sin^3\theta\cos\theta + (Q_{xy} - Q_{yy} + 2Q_{ss})\sin\theta\cos^3\theta \quad \cdots\cdots (14)$$

This transformation allowed us to express A_{ij}, B_{ij} and D_{ij} from classical lamination theory and elastic-viscoelastic correspondence principle as follows :

$$A^*_{ij} = A'_{ij} + iA''_{ij} = \sum_{k=1}^{N}(\overline{Q}'_{ij} + i\overline{Q}''_{ij})_{(k)}(h_k - h_{k-1}) \quad \cdots\cdots (15)$$

$$B^*_{ij} = B'_{ij} + iB''_{ij} = \frac{1}{2}\sum_{k=1}^{N}(\overline{Q}'_{ij} + i\overline{Q}''_{ij})_{(k)}(h_k^2 - h_{k-1}^2) \quad \cdots\cdots (16)$$

$$D^*_{ij} = D'_{ij} + iD''_{ij} = \frac{1}{3}\sum_{k=1}^{N}(\overline{Q}'_{ij} + i\overline{Q}''_{ij})_{(k)}(h_k^3 - h_{k-1}^3) \quad \cdots\cdots (17)$$

where, $i = \sqrt{-1}$. These effective modulus constants obtained on 2-D and 3-D textile structural models were converted to the corresponding complex modulus constants by using the elastic-viscoelastic correspondence principle to evaluate the dissipation constants. The material damping coefficients of 2-D and 3-D textile structural composites were then obtained as follows :

$$A\eta_{ij}(\text{stretching}) = A_{ij}''/A_{ij}' \quad \cdots\cdots (18)$$

$$B\eta_{ij}(\text{coupling}) = B_{ij}''/B_{ij}' \quad \cdots\cdots (19)$$

$$D\eta_{ij}(\text{bending}) = D_{ij}''/D_{ij}' \quad \cdots\cdots (20)$$

where, i, j= 1, 2, 6. Consequently, the effective laminate engineering constants E_1, E_2, υ_{12} and G_{12} can be expressed as functions of the stretching stiffness constants, A_{ij}, and the unit cell thickness. We obtained the material damping for 2-D woven and 3-D braided textile structural composites in terms of the physically measurable effective engineering properties, by evaluating the storage stiffness constants A_{ij} and the corresponding dissipation constants separately from the relationships between the effective engineering constants and [A] stiffness constants.

2-2. Mechanics of 2-D woven fabric composites

Two dimensional woven fabrics are generally constructed by the interlacing of fill and warp threads. The length direction of the fabric is defined as the warp, and the width direction is referred to as the fill or weft. Fabrics can be classified by the geometrical repeating pattern, denoted by ng, in non-hybrid fabrics, as shown in Fig.(1) (see Review in [12]).

2-2-1. Mosaic Model

The mosaic model represents a simplified description of the 2-D woven fabric by neglecting the thread crimp, as shown in Fig.(2). For the theoretical analysis in Fig.(2), the constitutive relationships can be written based upon classical laminated plate theory:

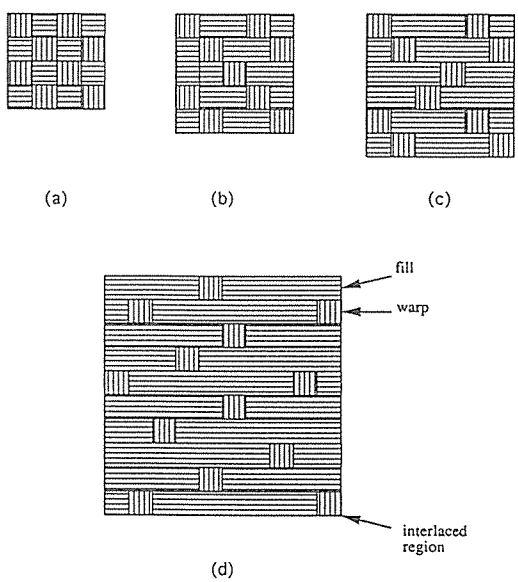

Fig. 1. Examples of Woven Fabric Patterns: (a) Plain Weave(ng=2) (b) Twill Weave(ng=3) (c) 4 Harness Satin (ng=4) (d) 8 Harness Satin (ng=8) [12].

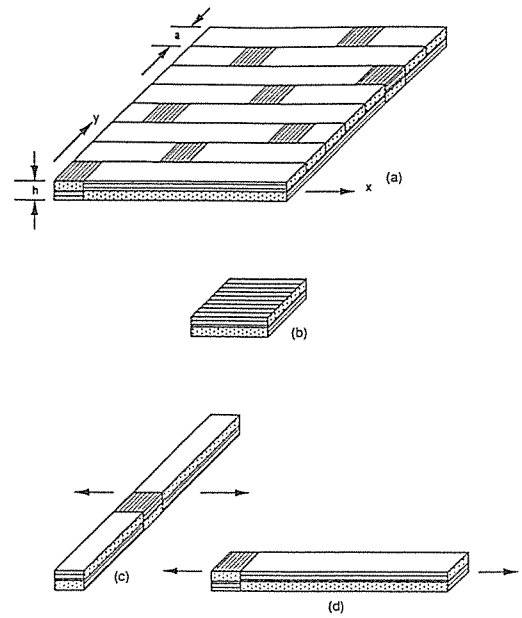

Fig. 2. Mosaic Model : (a) Repeating Region in an Eighth Harness Satin Compoaite (b) A Basic CrossPly Laminate (c) Parallel Model (d) Series Model [12].

$$\begin{pmatrix} N_i \\ M_i \end{pmatrix} = \begin{pmatrix} A_{ij} & B_{ij} \\ B_{ij} & D_{ij} \end{pmatrix} \begin{pmatrix} \varepsilon_{j^o} \\ k_j \end{pmatrix} \quad \cdots\cdots\cdots\cdots\cdots\cdots\cdots\cdots \quad (21)$$

Inverting Eq.(21), we obtained the following constitutive relationship :

$$\begin{pmatrix} \varepsilon_{i^o} \\ k_i \end{pmatrix} = \begin{pmatrix} a_{ij} & b_{ij} \\ b_{ij} & d_{ij} \end{pmatrix} \begin{pmatrix} N_j \\ M_j \end{pmatrix} = \quad \cdots\cdots\cdots\cdots\cdots\cdots\cdots\cdots \quad (22)$$

The upper and lower bounds of the static elastic moduli in these fabric composites were first introduced by Ishikawa and Chou[4,5]. By making the iso-stress and iso-strain assumptions, we determined the averaged static elastic properties in the repeating region of 2-D woven fabric composites using the procedures developed for conventional laminated

composites. The upper bounds of compliances, for instance, were obtained as

$$\bar{a}_{ij} = a_{ij}$$
$$\bar{b}_{ij} = (1 - \frac{2}{n_g})\, b_{ij} \quad \cdots\cdots (23)$$
$$\bar{d}_{ij} = d_{ij}$$

By inverting Eq.(23), the lower bounds of stiffnesses were obtained. Here, a_{ij}, b_{ij} and d_{ij} are determined from the equivalent cross ply laminate with unidirectional plies of the same volume fraction and total thickness of the fabric composite.

2-2-2. Crimp Model

The crimp model was proposed [4,5] to account for the continuity and undulations of fibers in a fabric composite. This model provides more accurate static elastic moduli for plain weave composites. Fig.(3) depicts the sinusoidal shape of the fill thread, the lenticular shape of the warp thread, and the cusp of matrix. We assumed that the laminated plate theory is applicable to each infinitesimal piece of the length dx along the x-direction. This assumption resulted in the following local in-plane stiffness of the fabric composites for the region[0, a/2]:

$$A_{ij}(x) = Q_{ij}^{M}[h_1(x) - h_2(x) + h + h_t/2] + Q_{ij}^{F}(\theta)h_t/2 + Q_{ij}^{W}[h_2(x) - h_1(x)] \quad \cdots\cdots (24)$$

where, the superscripts M, F and W indicate the pure matrix, fill and warp parts, respectively. The calculation of the off-axis stiffness, $Q_{ij}^{F}(\theta)$ is illustrated in Ref.[4]. We evaluated $B_{ij}(x)$ and $D_{ij}(x)$ by a similar approach. Thus, $a_{ij}(x)$, $b_{ij}(x)$ and $d_{ij}(x)$ were obtained by the inversion of the 6x6 matrix of the stiffness. The averaged in-plane compliance constants are expressed by

$$\bar{a}_{ij}^{C} = \frac{2}{n_g a}\int_0^{n_g a/2} a_{ij}(x)\, dx \quad \cdots\cdots (25)$$

where, the superscript C denotes the result of the crimp model. Finally, the averaged stiffness constants were determined by inverting $\bar{a}_{ij}^{C}$, $\bar{b}_{ij}^{C}$ and $\bar{d}_{ij}^{C}$.

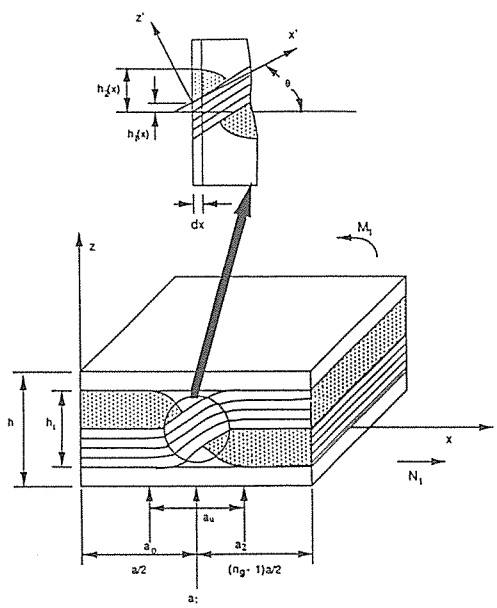

Fig. 3. Fiber Crimp Model [12].

2-2-3. Bridging Model

In the bridging model, the general satin weave is viewed as a combination of mosaic and crimp models. It is also assumed that the total in-plane force carried by region B, C and D is equivalent to that carried by region A or E in Fig. (4). Thus, the following averaged compliance constants were obtained:

$$\bar{a}_{ij}^{S} = \frac{1}{\sqrt{n_g}}\,[2\bar{a}_{ij} + (\sqrt{n_g - 2})\, a_{ij}] \quad \cdots\cdots (26)$$

The $\bar{b}_{ij}^{S}$ and $\bar{d}_{ij}^{S}$ could be similarly expressed. Here, $\bar{a}_{ij}$, $\bar{b}_{ij}$ and $\bar{d}_{ij}$ are the inverse of the av-

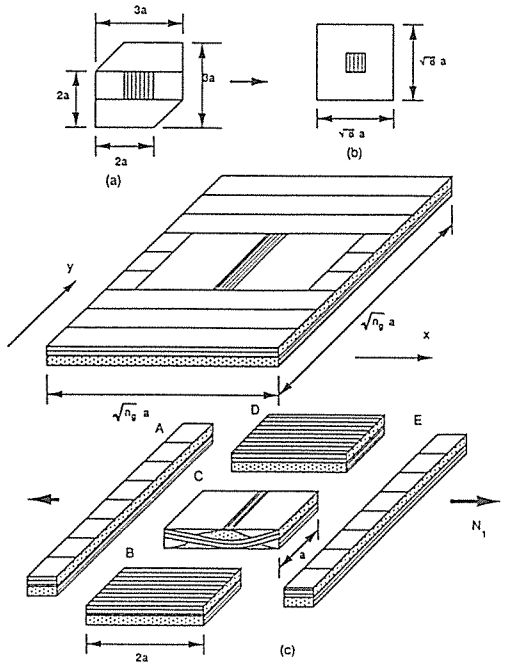

Fig. 4. Bridging Model: (a) Shape of the Repeating Unit of 8 Harness Satin (b) Modified Shape for the Repeating Unit (c) Idealization Concept for the Bridging Model [12].

erage stiffness constants for the regions B, C and D in the same formulation as in Eq.(26) and the terms with a superscript S denote properties of the entire satin plane. Consequently, $\overline{A}_{ij}^{S}$, $\overline{B}_{ij}^{S}$ and $\overline{D}_{ij}^{S}$ were obtained by inverting $\overline{a}_{ij}^{S}$, $\overline{b}_{ij}^{S}$ and $\overline{d}_{ij}^{S}$.

2-3. Mechanics of 3-D braided composites

The material properties of a three-dimensional braided composite depend on several factors such as fiber and matrix type, fiber volume fraction and yarn orientation. To analyze these material properties, the micro unit cell structure is defined by the length, w, width, u and thickness, v as shown in Fig. (5).

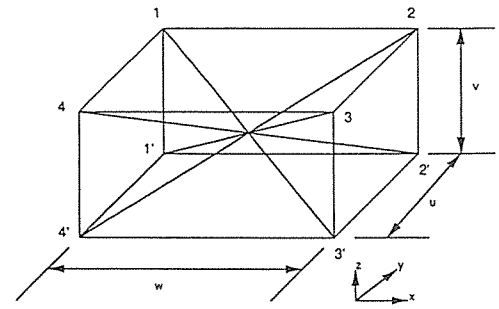

Fig. 5. The Unit Cell Structure of a 3-D Braided Structural Composite [8].

These geometric parameters are strongly dependent on the compacting and shedding motions when the braided preform is constructed [8]. The spatial yarn orientation may be defined as follows:

$$\theta = \tan^{-1}\frac{\sqrt{u^2+v^2}}{w} \quad \cdots\cdots (27)$$

An off-axis angle, $\theta_\beta = \tan^{-1}u/w$, with reference to the braiding axis, and the inclination angles, $\text{ehteta}_\alpha = \tan^{-1}\frac{v}{L}$, and $L = \sqrt{u^2+w^2}$, were also defined.

By accounting for the transverse isotropy in the ζ-ξmaterial plane perpendicular to the yarn direction, the stress-strain constitutive equations were expressed by [8]:

$$\begin{pmatrix}\sigma_\zeta\\ \sigma_\xi\\ \tau_{\zeta\xi}\end{pmatrix} = \begin{pmatrix}Q_{11} & Q_{12} & 0\\ Q_{12} & Q_{22} & 0\\ 0 & 0 & Q_{66}\end{pmatrix}\begin{pmatrix}\varepsilon_\zeta\\ \varepsilon_\xi\\ \gamma_{\zeta\xi}\end{pmatrix} \quad \cdots\cdots (28)$$

$$Q_{11} = \frac{E_\zeta(\theta_\alpha)}{1-\nu_{\zeta\xi}^2(\theta_\alpha)E_\xi(\theta_\alpha)/E_\zeta(\theta_\alpha)} \quad \cdots\cdots (29)$$

$$Q_{12} = \frac{\nu_{\zeta\xi}(\theta_\alpha)E_\zeta(\theta_\alpha)}{1-\nu_{\zeta\xi}^2(\theta_\alpha)E_\xi(\theta_\alpha)/E_\zeta(\theta_\alpha)} \quad \cdots\cdots (30)$$

$$Q_{22} = \frac{E_\xi(\theta_\alpha)}{1-\nu_{\zeta\xi}^2(\theta_\alpha)E_\xi(\theta_\alpha)/E_\zeta(\theta_\alpha)} \quad \cdots\cdots (31)$$

$$Q_{66} = G_{\zeta\zeta}(\theta_\alpha) \quad \cdots\cdots (32)$$

The yarn segments in an inclined lamina also form an off-axis angle, θ_β, with reference to the braiding direction (x-axis). Thus, the effective laminar elastic properties in the x-direction, when transformed by an off-axis angle θ_β, were expressed as $\overline{Q}_{ij}(\theta_\alpha, \theta_\beta)$. To obtain the [A, B, D] stiffness matrices, we integrated $\overline{Q}_{ij}(\theta_\alpha, \theta_\beta)$ for the lamina through the thickness of the unit cell of Fig.(6). However, we did not consider the effect of the pure matrix region in this model. We calculate stretching stiffness A_{ij} as [8]:

$$A_{ij}(x) = \int_{H_1(\zeta_1)}^{H_1(\zeta_1)+h'} \overline{Q}_{ij}^{(1)}(\theta_\alpha, \theta_\beta)\, dz + \int_{H_2(\zeta_2)-h'}^{H_2(\zeta_2)} \overline{Q}_{ij}^{(2)}(\theta_\alpha, \theta_\beta) dz + \int_{H_3(\zeta_1)}^{H_3(\zeta_1)+h'} \overline{Q}_{ij}^{(3)}(\theta_\alpha, \theta_\beta)\, dz + \int_{H_4(\zeta_2)-h'}^{H_4(\zeta_2)} \overline{Q}_{ij}^{(4)}(\theta_\alpha, \theta_\beta)\, dz \quad \cdots\cdots (33)$$

where, $h' = \dfrac{h}{\cos\theta_\alpha}$; h is the lamina thickness with the following constraints :

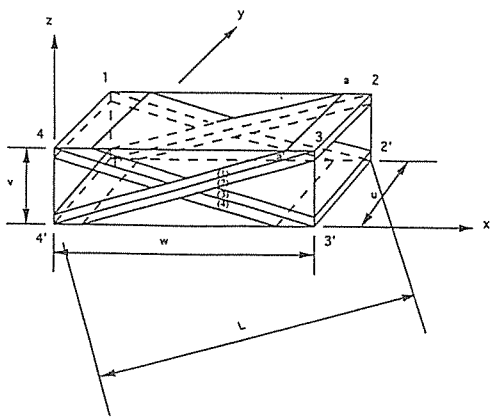

Fig. 6. The Unit Cell of the Fiber Inclination Model Composed of Four Unidirectional Laminae [8].

$\overline{Q}_{ij}^{(1)}(\theta_\alpha, \theta_\beta) : \theta_\alpha > 0$ and $\theta_\beta < 0$

$\overline{Q}_{ij}^{(2)}(\theta_\alpha, \theta_\beta) : \theta_\alpha > 0$ and $\theta_\beta < 0$

$\overline{Q}_{ij}^{(3)}(\theta_\alpha, \theta_\beta) : \theta_\alpha > 0$ and $\theta_\beta < 0$

$\overline{Q}_{ij}^{(4)}(\theta_\alpha, \theta_\beta) : \theta_\alpha > 0$ and $\theta_\beta < 0$

$B_{ij}(x)$ and $D_{ij}(x)$ were similarly evaluated. The variable h, defined as the total cross-sectional area of the laminae (1), (2), (3) and (4) in the xz plane, was set equal to that of the unit cell. In order to determine the average stiffness in the unit cell, we evaluated the local laminate compliance matrices $a_{ij}(x)$, $b_{ij}(x)$ and $d_{ij}(x)$ by inverting the local stiffness matrices $A_{ij}(x)$, $B_{ij}(x)$ and $D_{ij}(x)$. The average in-plane compliance of the unit cell under a uniform in-plane loading is

$$\overline{a}_{ij} = \frac{1}{w}\int_0^w a_{ij}(x)\, dx \quad \cdots\cdots (34)$$

and, $\overline{b}_{ij}$ and $\overline{d}_{ij}$ were similarly expressed.

Consequently, the average stiffness matrices $\overline{A}_{ij}$, $\overline{B}_{ij}$ and $\overline{D}_{ij}$ for the unit cell were determined by taking the inverse of $\overline{a}_{ij}$, $\overline{b}_{ij}$ and $\overline{d}_{ij}$.

3. EXPERIMENTAL

3-1. Experimental Setup

Figure (7) shows a schematic of an improved experimental setup for measuring the damping of a 2-D textile structural composite beam. The beam specimen was excited by means of an electrodynamic exciter driven by a random noise generator [13]. The exciter was a mini-shaker (Bruel & Kjaer 4810). To obtain double cantilever support, the specimen was mounted at its center directly on the impedance head using a 1-mm width thin strip of double-sided adhesive tape.

The impedance head (Bruel & Kjaer 8000) was mounted on the exciter and it directly measured the acceleration response and the in-

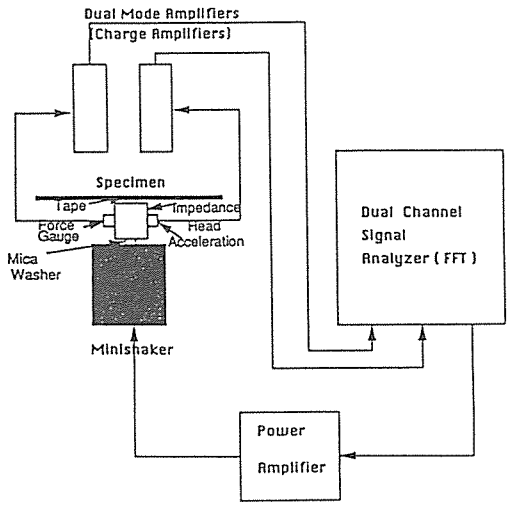

Fig. 7. Improved Experimental Setup for Measurement of Material Damping.

put force of the beam specimen. A dual channel signal analyzer (Bruel & Kjaer 2032) was used to determine the frequency response function from the force and acceleration signals of the impedance head connected to the specimen. The damping value for each of the specimens was measured by using the half power bandwidth method in a zoom mode of the frequency response of the specimen.

3-2. Specimen Fabrication

The 2-D fabric composite specimens investigated were of identical zbeams trimmed from plates that were made with desired structural geometric parameters. The 2-D fabric composite plates were fabricated from 2-4 layers of graphite fabric preforms impregnated with epoxy resin (Epon 826) and Z hardener. The graphite textile structural preforms used were plain weave, 4 harness, 5 harness and 8 harness satin weave fabrics woven from polyacrylonitrite (PAN) based carbon yarns (3K and 6K-filament-count continuous AS4 fibers). The graphite yarn had fiber bundle thickness, strength, Young's modulus, and ultimate elongation of 0.21 or 0.42mm, 3.5 GPa, 235 GPa and 1.03 %, respectively. The lay-up was subjected to compression molding at 80 PSI and 80℃ for 2 hours. After compression molding, it was also subjected to post curing at 150℃ for 2 hours. The beam specimens of dimensions 19. 05 X 2.54 X 0.0762 cm were machined from these fabricated plates.

Ⅳ. RESULTS AND DISCUSSION

The theoretical damping values of [A], [B] and [D] were determined by first expressing [A], [B], and [D] by the stiffness matrix $[Q]_k$ and layer thickness hk of each laminate. In addition, we employed the relations of Q_{ij}^k in terms of the 4 basic engineering constants E_L, E_T, G_{LT} and υ_{LT}. To determine the stretching damping ($A\eta_{ij} = A_{ij}''/A_{ij}'$), coupling damping ($B\eta_{ij} = B_{ij}''/B_{ij}'$), bending damping ($D\eta_{ij} = D_{ij}''/D_{ij}'$) and effective engineering damping, we must also substitute the basic engineering constants into the complex moduli using the elastic and viscoelastic correspondence principle. In this study, the basic damping factors ηL, ηT, ηLT, $\eta\upsilon$LT were obtained based on the Modified Hashin's theory and Rule-of-Mixture Laws. In Figs.(8)-(20), the physical quantities were described as;

$A\eta_{11}$: extensional damping along the axis of 1
$A\eta_{12}$: extensional damping along the axis of 2
$A\eta_{66}$: in-plane shear damping
$B\eta_{11}$: coupling damping along the axis of 1
$D\eta_{11}$: flexural damping along the axis of 1
$D\eta_{12}$: flexural damping along the axis of 2
$D\eta_{66}$: flexural shear damping
ηE_{11} : effective in-plane axial damping
ηG_{12} : effective in-plane shear damping
$\eta\upsilon_{12}$: effective in-plane Poisson's damping

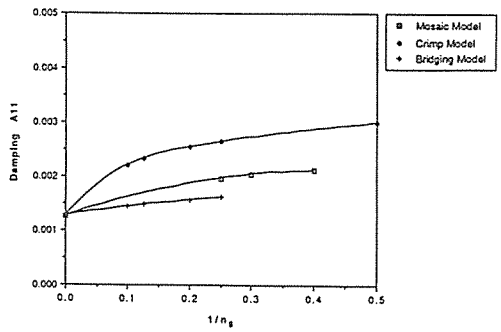

Fig. 8. Variations of Damping A_{11} with 1/ng.

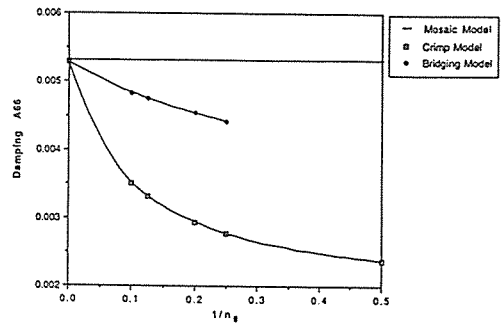

Fig. 10. Variations of Damping A_{66} with 1/ng.

For 2-D woven fabric composites, numerical results for the above quantities are presented in Figs.(8)-(17). Plots of $A\eta_{11}$, $B\eta_{11}$, $D\eta_{11}$ and ηE_{11} of the lower limit of the models for 2-D textile structural composites as a function of ng are illustrated in Figs.(8), (11), (12) and (15). These figures show that the damping increased with decreasing value of ng, probably due to fiber undulation. In other words, damping increased with increasing fiber undulation in these textile structural composites. Different behaviors were exhibited in the bridging model (Figs.(9) and (17)). Their damping values increased with increasing value of ng. Damping along the 1-direction was greater than that along the 2-direction (Figs.(8)(9), (12) (13)). Figs.(10), (14) and (16) show that values of $A\eta_{66}$, $D\eta_{66}$ and ηG_{12} either remained constant or decreased as the value of ng decreased.

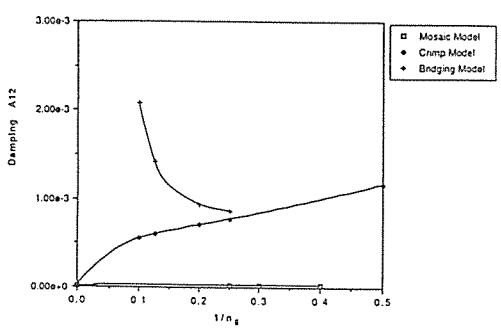

Fig. 9. Variations of Damping A_{12} with 1/ng.

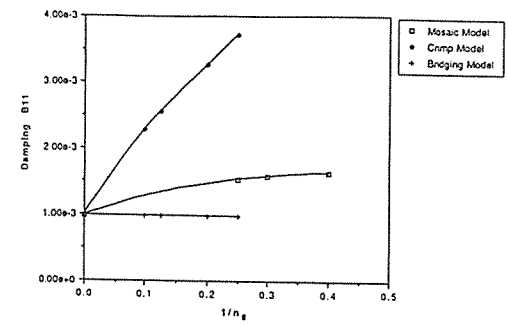

Fig. 11. Variations of Damping B_{11} with 1/ng.

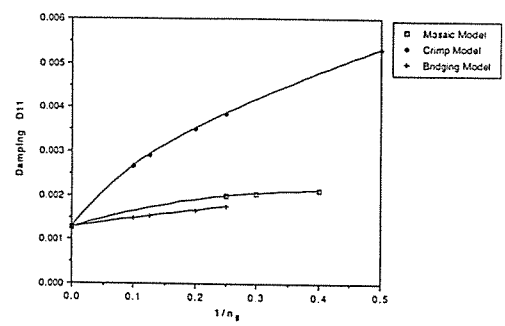

Fig. 12. Variations of Damping D_{11} with 1/ng.

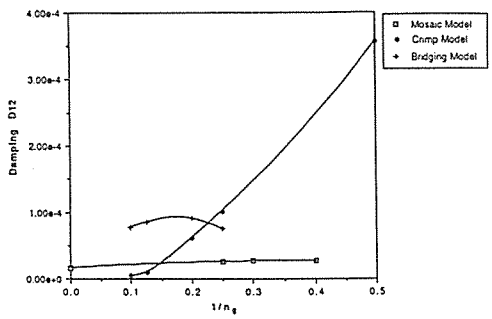

Fig. 13. Variations of Damping D_{12} with 1/ng.

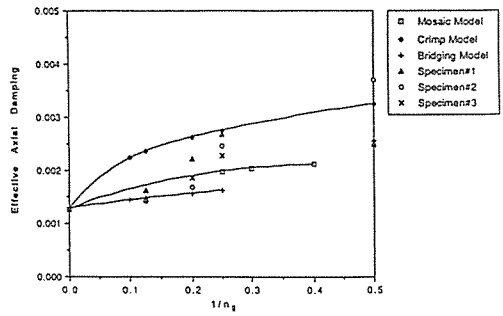

Fig. 15. Variations of Damping E_{11} with 1/ng.

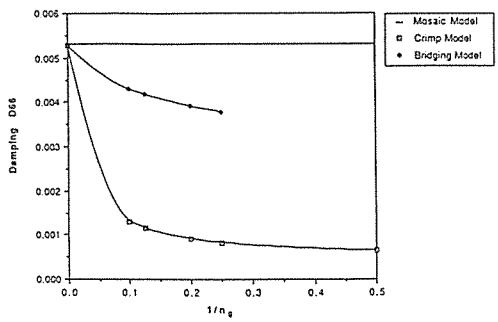

Fig. 14. Variations of Damping D_{66} with 1/ng.

Experimental confirmation of 2-D woven fabric composites has been conducted. Experimental results of the effective damping, ηE_{11}, showed a reasonable agreement with theoretical values (Fig.(15)), even though it is very difficult to make precise measurements. The discrepancy between experimental results and theoretical values may be caused by the effect of different gaps between two adjacent yarns, different fiber bundle sizes, and different laminate configuration with different number of layers. Numerical calculations showed that ηE_{11} was of the same value as $A\eta_{11}$, and ηG_{12} was of the same value as Ah66. It was found that stretching damping values ($A\eta_{11}$) were almost the same as flexural damping values ($D\eta_{11}$) in Mosaic and Bridging Models of 2-D woven textile structural composites. These results demonstrated that stretching damping, stretching-bending coupling damping, bending damping, in-plane axial damping, in-plane shear damping and in-plane Poisson's damping are all functions of ng (a geometric parameter) in 2-D textile structural composites. The lower limit values on the damping loss factor may provide useful information as a material property for design purposes.

For 3-D braided textile structural composites, numerical calculations were performed for the graphite preform in epoxy resin. The basic material properties used were E_f=235 GPa and υ_f=0.22 for 12k graphite fiber, E_m=4.3 GPa and υ_m=0.34 for epoxy resin. The geometric parameters u, v and w were specifically employed based upon the unit cell of 3-D braided plain weave composites which Whitney [11] measured. The w is a function of the compacting motion during the preform construction. The average yarn orientation angle decreases with increasing w. An increase of the w value from 3.5 mm to 6.5 mm brings about a decrease of the yarn angle by about 12°. Numerical results are presented in Figs. (18), (19) and (20), which clearly show that damping was a function of fiber volume fraction and yarn orientation. Fig.(18) demonstrates that the axial damping was significantly influenced

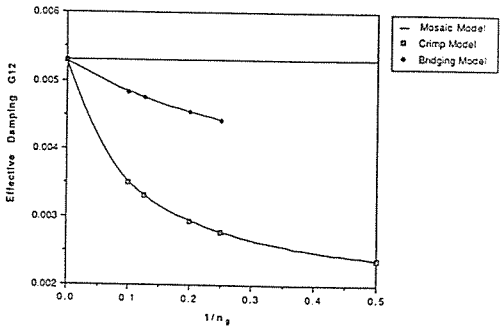

Fig. 16. Variations of Damping G_{12} with 1/ng.

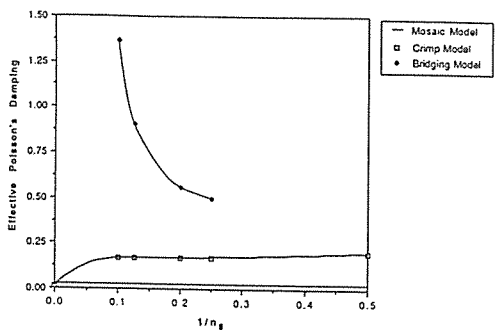

Fig. 17. Variations of Poisson's damping with 1/ng.

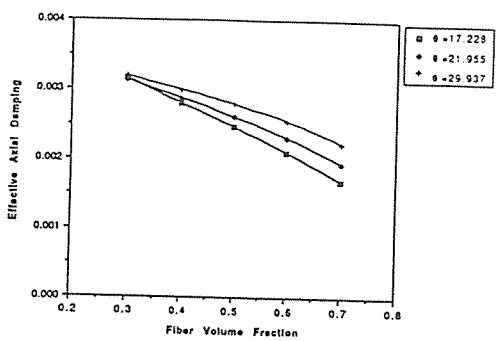

Fig. 18. Predicted Damping E_{11} of 3-D braided graphite/epoxy composites as functions of fiber volume fraction and spatial yarn orientation.

by the yarn orientation angle and fiber volume fraction. For a fixed fiber volume fraction, as the braiding angle became greater, the axial damping also became greater. Also, the axial damping decreases with increasing fiber volume fraction. Since materials with higher damping are usually characterized by lower stiffness, the damping behavior of axial stiffness in Fig.(18) was opposite to the corresponding axial stiffness data observed by Yang [8]. Fig.(19) demonstrates that the predicted in-plane shear damping was as a function of the fiber volume fraction and yarn orientation. The in-plane shear damping was little affected by the fiber inclination angle. Fig.(20) illustrates the results of in-plane Poisson's damping. For the variations of fiber

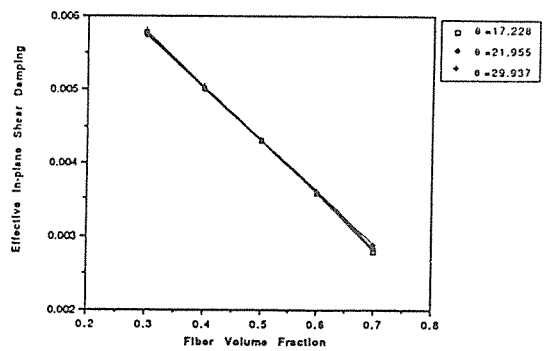

Fig. 19. Predicted Damping G_{12} of 3-D braided graphite/epoxy composites as functions of fiber volume fraction and spatial yarn orientation.

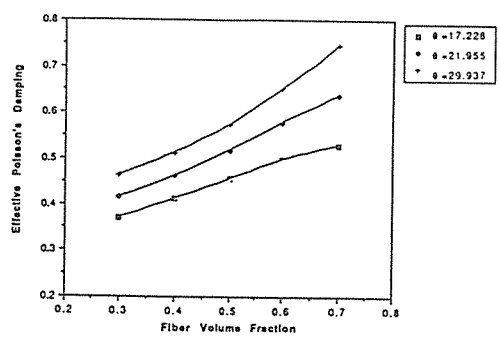

Fig. 20. Predicted Poisson's damping of 3-D braided graphite/epoxy composites as functions of fiber volume fraction and spatial yarn orientation.

volume fraction, the behavior of the in-plane Possion's damping was opposite to the corresponding axial damping and it increased with increasing fiber volume fraction.

CONCLUDING REMARKS

(1) A methodology for predicting the damping properties of 2-D and 3-D textile structural composites was developed based upon existing models for various static moduli, a modified lamination theory and the elastic-viscoelastic correspondence principle.

(2) Stretching damping, coupling damping, bending damping, axial damping, Poisson's damping and in-plane shear damping are all functions of ng (a geometric parameter) in 2-D woven textile structural composites.

(3) Based upon the obtained numerical results, lower bound solutions provided realistic values of damping in a 2-D woven fabric composites. The damping values may be considered a material property in these fabric composites for design purposes.

(4) Damping in 3-D braided composites was significantly influnced by the fiber volume fraction and yarn orientation angle.

LIST OF SYMBOLS

$[A]$ = 3x3 extensional stiffness matrices
$[B]$ = 3x3 coupling stiffness matrices
$[D]$ = 3x3 bending stiffness matrices
$[Q]_k$ = 3x3 laminate modulus matrices
Q_{ij}^k = laminate modulus components
E_L = extensional modulus for the 0° composite
E_T = transverse modulus for the 0° composite
G_{LT} = in-plane shear modulus for the 0° composite
υ_{LT} = in-plane Poisson's ratio for the 0° composite
A_{ij}', A_{ij}'' = extensional storage and loss stiffness for the composite
B_{ij}', B_{ij}'' = coupling storage and loss stiffness for the composite
D_{ij}', D_{ij}'' = bending storage and loss stiffness for the composite
$A\eta_{ij}$ = extensional damping
$B\eta_{ij}$ = coupling damping
$D\eta_{ij}$ = bending damping
ηE_{11} = effective in-plane axial damping
ηG_{12} = effective in-plane shear damping
$\eta\upsilon_{12}$ = effective in-plane Poisson's damping
E_L^* = extensional complex modulus for the 0° composite
E_T^* = transverse complex modulus for the 0° composite
G_{LT}^* = in-plane shear complex modulus for the 0° composite
υ_{LT}^* = in-plane complex Poisson's ratio for the 0° composite
η_L = basic axial damping for the 0° composite
η_T = basic transverse damping for the 0° composite
η_{LT} = basic in-plane shear damping for the 0° composite
$\eta\upsilon_{LT}$ = basic in-plane Poisson's damping for the 0° composite
V_m = matrix volume fraction
V_f = fiber volume fraction
η_m = matrix damping
E_{Lf} = axial modulus for the fiber
E_m = matrix Young's modulus
E_{Tf} = transverse modulus for the fiber
G_f = in-plane shear modulus for the fiber
G_m = matrix shear modulus
$\upsilon_{LTf}(\upsilon_f)$ = fiber Poisson's ratio
$\upsilon_{LTm}(\upsilon_m)$ = matrix Poisson's ratio
α, ζ, β = curve fitting parameters
Q_{xx}, Q_{xy}, Q_{yy}, and Q_{ss} = 0° laminate modulus components
Q_{xx}^*, Q_{xy}^*, Q_{yy}^* and Q_{ss}^* = 0° laminate complex modulus components
Q_{xx}', Q_{xy}', Q_{yy}', Q_{ss}' and Q_{xx}'', Q_{xy}'', Q_{yy}'', Q_{ss}'' = 0° laminate storage and loss modulus components

$\overline{Q}'_{ij}$ and $\overline{Q}''_{ij}$ = transformed laminate storage and loss modulus components for the off-axis composite
k = layer number
h = laminate thickness
h_k = layer thickness
E_1 = effective axial modulus for the composite
E_2 = effective transverse modulus for 0° composite
G_{12} = effective in-plane shear modulus for 0° composite
υ_{12} = effective in-plane Poisson's ratio for 0° composite
N_i = stress resultants
M_i = stress couplings
ε^0 = strain components
κ = curvature components
a_{ij} = axial compliance stiffness components
b_{ij} = coupling compliance stiffness components
d_{ij} = bending compliance stiffness components
$\overline{a}_{ij}$ = average axial compliance stiffness components
$\overline{b}_{ij}$ = average coupling compliance stiffness components
$\overline{d}_{ij}$ = average bending compliance stiffness components
n_g = geometric parameter for the 2-D woven composite
u, v, w = unit cell dimension for the 3-D braided composite
θ = spatial yarn orientation
θ_β = off-axis angle
θ_α = inclination angle
i = $\sqrt{-1}$

Subscripts and Superscripts
1, 2, 6 = off-axis coordinate system
x, y, s = fiber coordinate system
M,F,W,C,S = matrix, fill, warp, crimp model and entire satin plane
$\overline{\ }$ = average property
* = complex property

ACKNOWLEDGMENTS

The support for this project was provided by the NSF/Alabama EPSCOR program to which we are grateful.

REFERENCES

1. Adams, R.D., "Damping Properties Analysis of Composites," Engineering Materials Handbook, Composites, Vol. 1, pp.206-217, ASM(1987).

2. Hashin, Z., "Complex Moduli of Viscoelastic Composites: II. Fiber Reinforced Materials," Int. J. Solids and Struc., Vol. 6, pp. 797-807(1970).

3. Sun, C.T., Wu, J.K. and Gibson, R.F., " Prediction of Material Damping of Laminated Polymer Matrix Composites," Journal of Materials and Science Vol. 22.(1987) pp.1006-1012.

4. Ishikawa, T. and Chou, T. W., "One-Dimensional Micromechanical Analysis of Woven Fabric Composites," AIAA Journal Vol. 21, No. 12, pp.1714-1721 (Dec.1983).

5. Ishikawa, T. and Chou, T. W., "Stiffness and Strength Behavior of Woven Fabric Composites," Journal of Materials and Science, Vol. 17, No. 11, pp.3211-3220 (Nov.1982).

6. Ishikawa, T., "Anti-Symmetric Elastic Properties of Composite Plates of Satin Weave Cloth," Fiber Science and Technology Vol. 15, pp.127-145 (Sep. 1981).

7. Ishikawa, T., Matsushima, M. and Hayashi, Y and Chou, T. W., "Experimental Confirmation of the Theory of Elastic Moduli of Fabric Composites," Journal of Composite Materials, Vol. 19, pp.443-458, Sep. 1985.

8. Yang, J. M., Ma, C.L. and Chou, T. W., " Fiber Inclination Model of Three Dimensional

Textile Structural Composites," Journal of Composite Materials, 20 (Sep. 1986) pp.472-484.

9. Ko, F.K. and Pastore, C.M. , "Structure and Properties of an Integrated 3D fabric for Structural Composites," J.R. Vinson and M. Taya, Ed., ASTM STP 864 (pp.428-439), American Society for Testing and Materials, Philadelpia, PA, 1985.

10. Ma, C.L., Yang, J.M. and Chou, T.W., "Elastic Stiffness of Three-dimensional braided Textile Structural Composites," J. M. Whitney, Ed., ASTM STP 893, 1986, pp.404-421.

11. Whitney, T.J. and Chou, T.W., "Modeling of 3-D Angle-Interlock Textile Structural Composites," Journal of Composite Materials 23(Sep. 1989) pp.890-911.

12. Chou, T.W. and Ko, F.K., "Textile Structural Composites," Composite Material Series, Vol. 3, 1989, pp.209-239.

13. Suarez, S.A., Gibson, R.F., and Deobold, L.R., "Random and Impulse Techniques for Measurements of Damping in Composite Materials," Experimental Techniques, Vol. 8, No. 10, Oct. 1984, pp.19-24.

14. Jones, R.M., "Mechanics of Composite Materials," Scripta Book Company, Washington, D.C., 1974.